Electronic Supplementary Material (ESI) for Nanoscale.

Supporting Information

$Ti_3C_2T_x$ nanosheet wrapped core-shell MnO_2 nanorods @ hollow porous carbon as a multifunctional polysulfide mediator for improved Li–S battery

Heng Zhang,‡ [a] Peigen Zhang,‡ [a] Long Pan,*[a] Wei He,[a] Qi Qi,[a] Li Yang,[a] Zhuoheng Bao,[a] Wei Zhang,[a] Michel W. Barsoum,[b] and ZhengMing Sun*[a]

[a] *Key Laboratory of Advanced Metallic Materials of Jiangsu Province, School of Materials Science and Engineering, Southeast University, Nanjing, 211189, China*

[b] *Department of Materials Science and Engineering, Drexel University, PA19104, USA*

* *Corresponding authors: zmsun@seu.edu.cn (Z.M. S.), panlong@seu.edu.cn (L. P.)*

‡ *These two authors are equal major contributors to this work.*

Table of Contents

1. Supplementary Figures

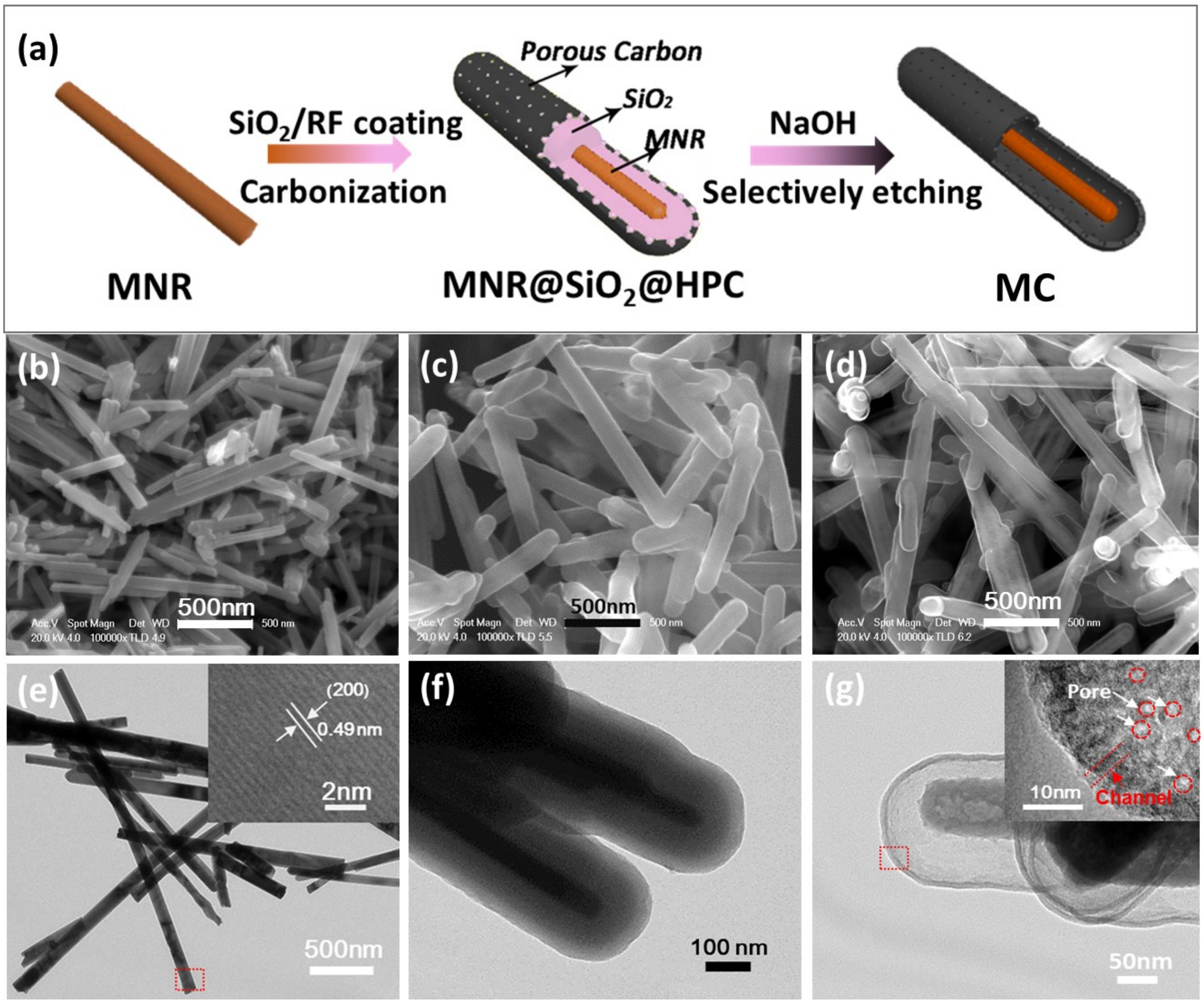

Fig. S1. (a) Schematic illustration for synthesis process of core-shell MC. (b-d) SEM images of MNR, MNR@SiO_2@HPC, and MC. (e-g) TEM images of (e) MNR, (f) MNR@SiO_2@C and (g) MC.

SEM and TEM images show the MnO_2 nanorods (MNR) have a homogenous lateral size distribution with an average diameter of ~50 nm, and their length scales are in the range of several microns. HRTEM image in the inset of (e) shows that MNR exhibits distinct lattice spacing of 0.49 nm corresponding to the (200) plane of MnO_2 (JCPDS No. 72-1982). After coating with SiO_2 and HPC layers, the average diameter of MNR@SiO_2@HPC is increased to about 200 nm. By etching the SiO_2 interlayer, the resulting MC shows a yolk-shell structure, in which the morphology of MNR and HPC are well preserved. HRTEM image in the inset of (g) indicates that the HPC shell with a thickness of about 10 nm contains a large number of mesopores with pore size of 3-4 nm. These pores can provide abundant channels for molten sulfur impregnation and Li ion diffusion.

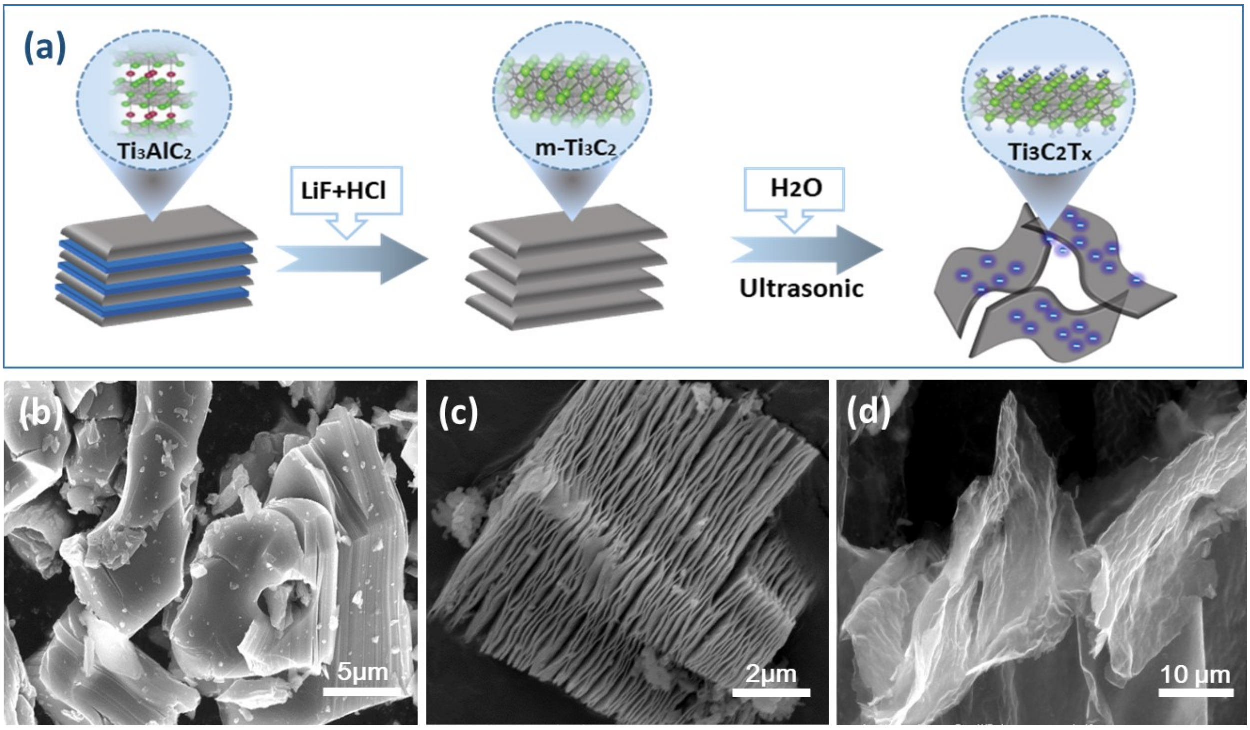

Fig. S2. (a) Schematic illustration for the synthesis process of $Ti_3C_2T_x$. (b-d) SEM images of MAX (Ti_3AlC_2), multilayered-$Ti_3C_2T_x$ (m-$Ti_3C_2T_x$), and $Ti_3C_2T_x$ nanosheets.

After etching Al atom layers from the dense layered Ti_3AlC_2 bulks, the m-$Ti_3C_2T_x$ with a typical accordion structure is further delaminated into few-layered, crumpled $Ti_3C_2T_x$ nanosheets *via* a simple, ultrasonic-assisted liquid exfoliation process.

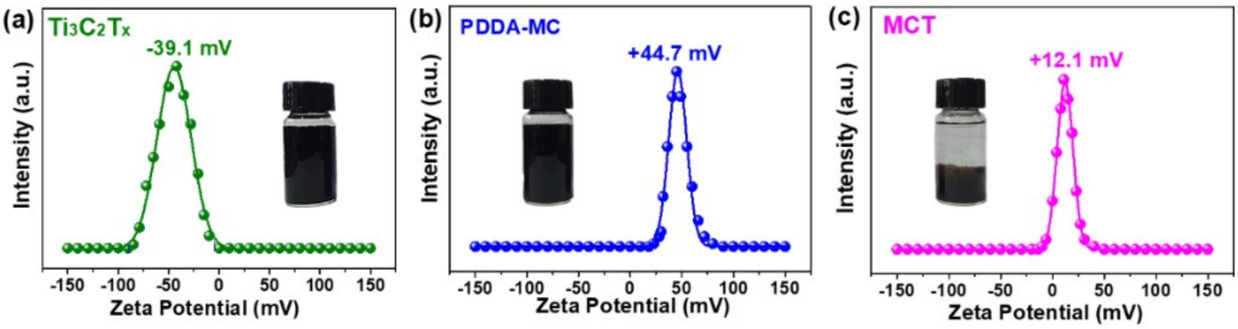

Fig. S3. Zeta-potential of (a) $Ti_3C_2T_x$, (b) PDDA-MC and (c) MCT. The insets are the photographs of the corresponding suspensions.

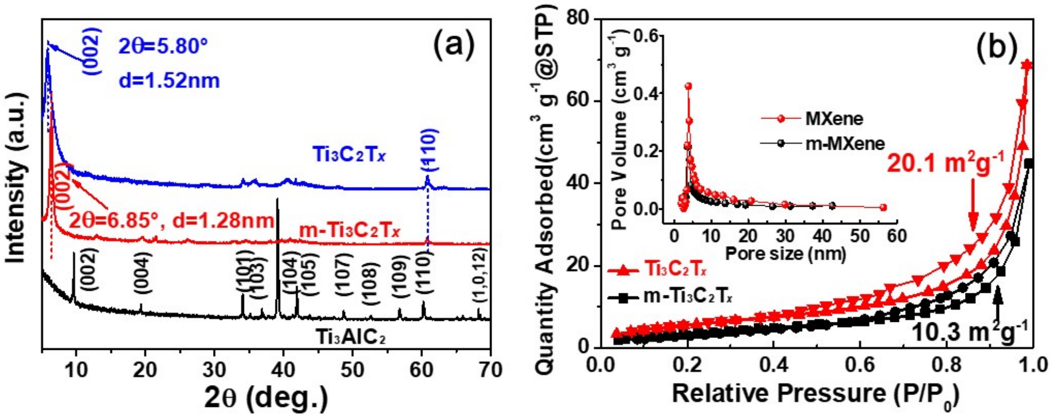

Fig. S4. (a) XRD patterns of Ti_3AlC_2 MAX, m-$Ti_3C_2T_x$ and $Ti_3C_2T_x$. (b) Nitrogen adsorption/desorption isotherms of m-$Ti_3C_2T_x$ and $Ti_3C_2T_x$. Inset of (b) is the corresponding pore size distributions.

In the XRD patterns, the most prominent (002) reflection of m-$Ti_3C_2T_x$ located at 6.85° shifts to a lower 2θ angle of 5.8° in the $Ti_3C_2T_x$, resulting in $Ti_3C_2T_x$ nanosheets have an bigger lattice spacing and more active sites than m-$Ti_3C_2T_x$.

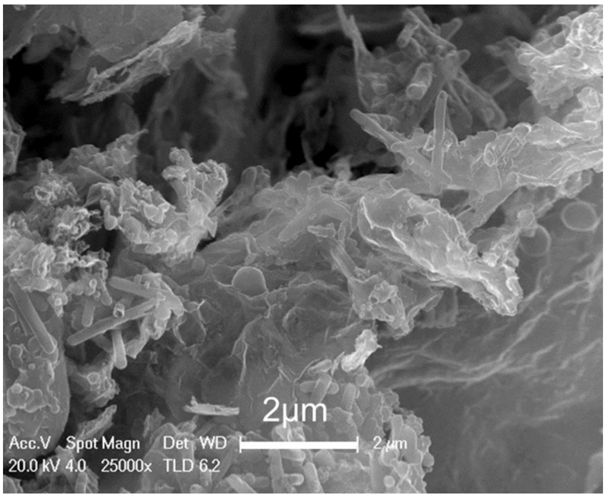

Fig. S5. SEM image of the 3D MCT hierarchical structure.

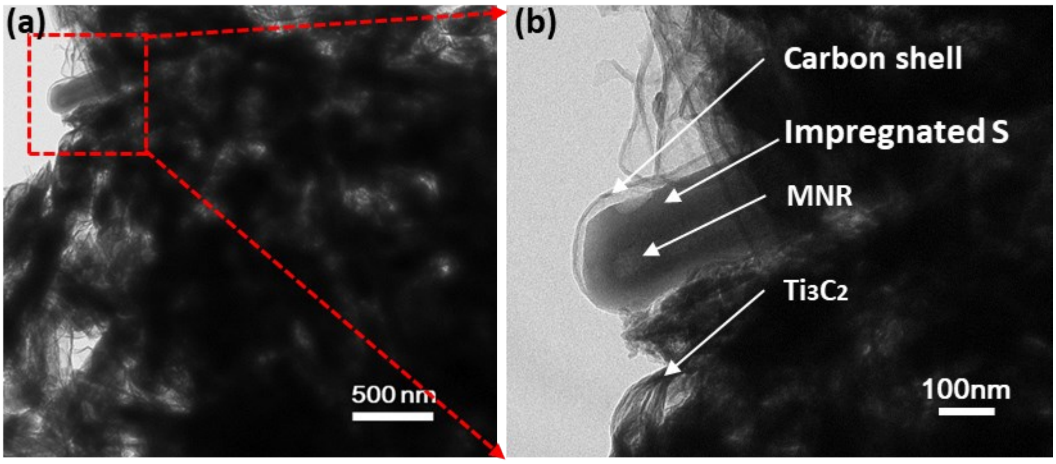

Fig. S6. (a, b) TEM images of the MCT/S composite.

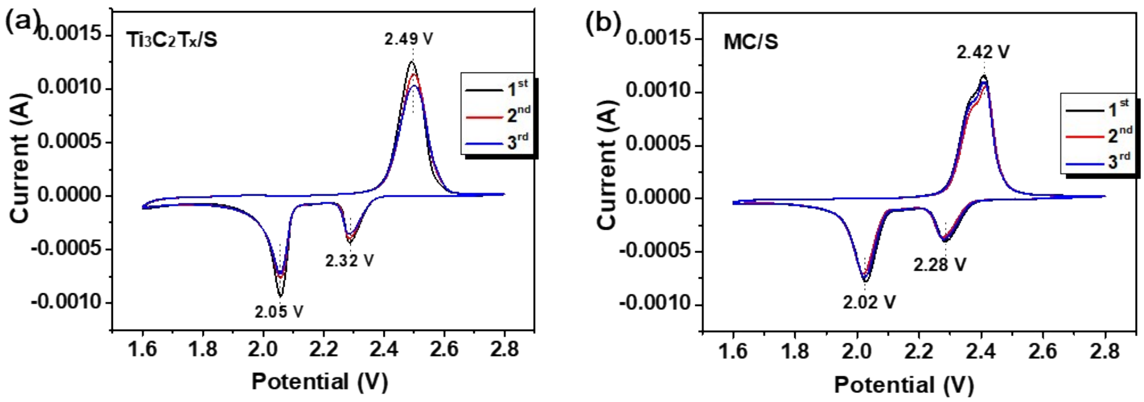

Fig. S7. (a, b) CV curves of the $Ti_3C_2T_x$/S and MC/S cathodes at 0.1 mV s^{-1}.

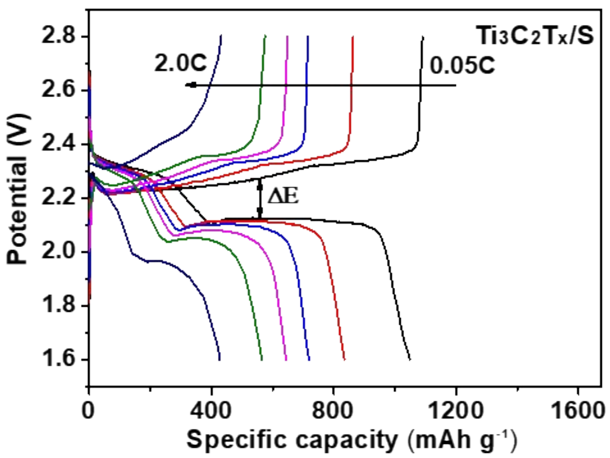

Fig. S8. Charging/discharging curves of the $Ti_3C_2T_x$/S cathode at different current densities.

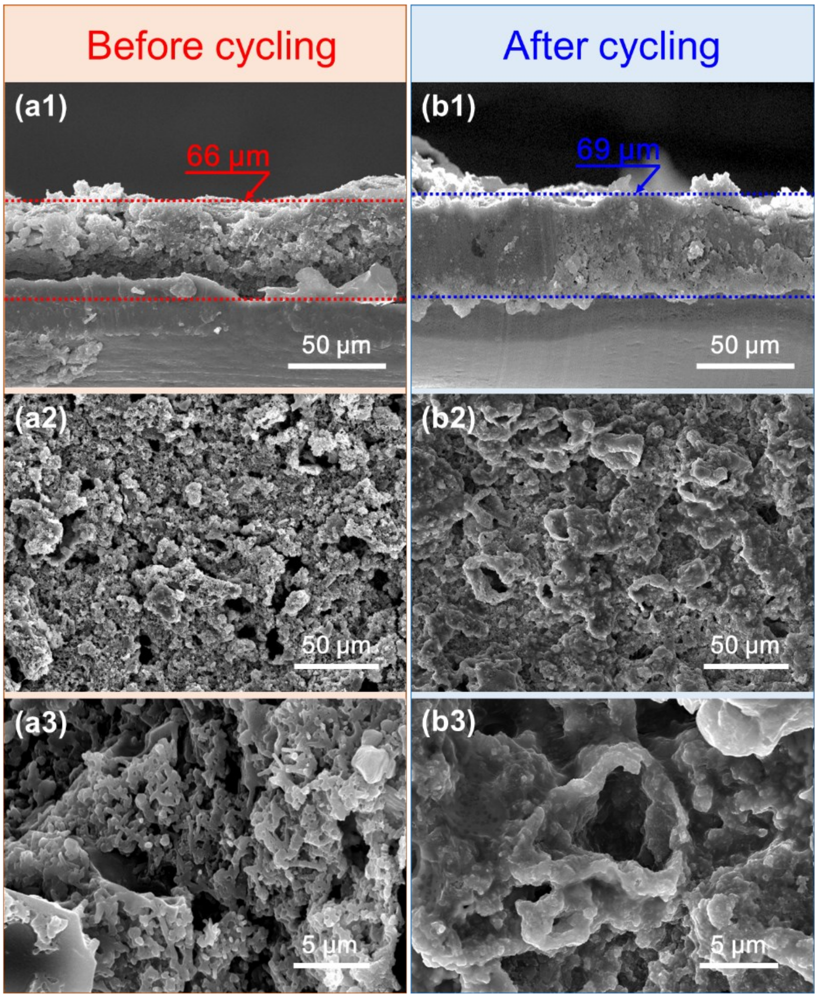

Fig. S9. SEM images of MCT/S electrode before (a) and after (b) cycling (200 cycles at 0.2C with a S-mass loading of 4.15 mg cm^{-2}). (a1, b1) Cross section and (a2-b3) top-view SEM images.

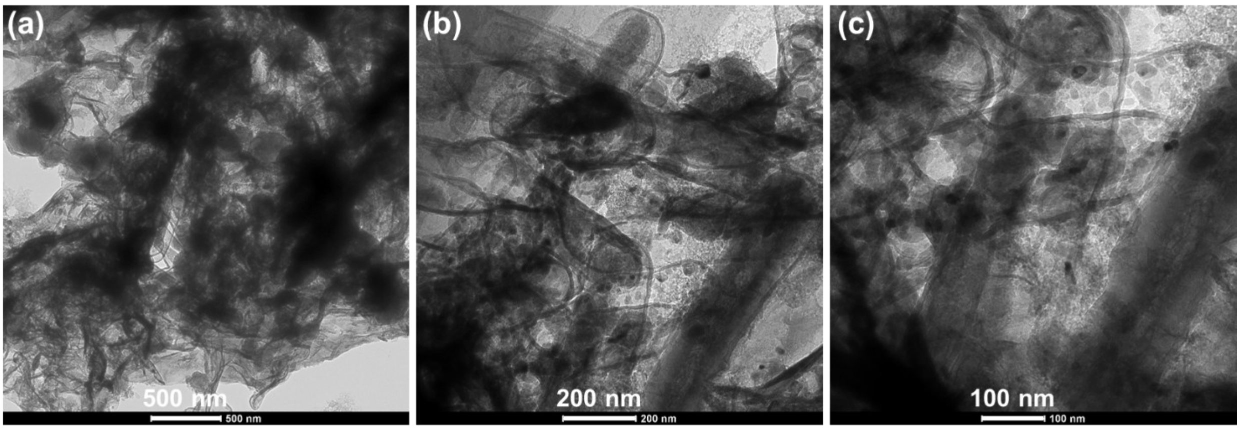

Fig. S10. TEM images at different magnification of MCT/S after cycling (200 cycles at 0.2C with a S-mass loading of 4.15 mg cm^{-2}).

2. Supplementary Tables

Table S1. Comparison of EIS fitting parameters in the equivalent circuit model for MCT/S, MC/S, and $Ti_3C_2T_x$/S cathodes

Cathodes	**R_e (Ω)**	**R_{ct} (Ω)**	**CPE_1**		**CPE_2**	
			Z_{CPE1} (Ω)	**n_1**	**Z_{CPE2} (Ω)**	**n_2**
MCT/S	2.50	24.28	5.10×10^2	0.66	29.02	0.57
MC/S	4.28	66.85	3.45×10^3	0.53	40.81	0.40
$Ti_3C_2T_x$/S	3.06	50.93	1.68×10^3	0.71	38.17	0.63

Z_{CPE} is defined as $Z_{CPE} = Y^{-1}(jw)^{-n}$. When $n = 1$, CPE represents an ideal capacitor with the capacitance Y; when $n = 0$, CPE is a resistor with the admittance Y.

Table S2. Comparisons among some other advanced sulfur cathodes for Li–S Batteries

Cathodes	Host feature	S content/loading (%/mg cm^{-2})	Initial capacity (mA h g^{-1}/C)	Rate capacity (mA h g^{-1}/C)	Cycle life (mA h g^{-1}/cycles/C)	Capacity decay (% per cycle)	Ref.
MCT/S	**3D hierarchical structure**	**75/2.0**	**1406/0.05**	**740/1.0** **688/2.0**	**953/200/1.0** **591/600/2.0**	**0.059** **0.044**	**This work**
rGO/MnO_2/S	Aerogel	67/0.8	1072/0.2	659/1.6	887/200/0.2	0.071	[1]
MnO_2@MXene/S	Aerogel	70/1.2	1140/0.05	615/2.0	731/500/1.0	0.06	[2]
MnO_2/NHCS/S	Nano-spheres	72/1.9	1283/0.2	1130/1.0	1283/500/0.2	0.067	[3]
MnO_2@GO/S	Double-shelled	52/0.6	976/0.02	269/1.5	1160/400/0.35	~0.14	[4]
MnO_2/GO/CNT/S	3D architecture	80/2.8	1500/0.05	960/1.0	963/100/0.2	0.162	[5]
Ti_3C_2/CF/S	3D framework	71/1.2	1380/0.1	510/5.0	581/1000/1.0	0.044	[6]
Ti_3C_2/rGO/ S	3D hybrid	70.4%/1.5	1190/0.2	923/2.0	1144/300/0.5	~0.077	[7]
Ti_3C_2/CNT/S	Interwoven	83/1.5	1216/0.05	1216/0.05	930/1200/0.5	0.043	[8]
TiO_2@Ti_3C_2/S	Nanosheets	80/1.5	1158/0.2	663/2.0	850/500/2.0	0.04	[9]
Ti_3C_2@PDA/S	Particle	78/5.0	1197/0.5	590/2.0	1000/1000/0.2	0.035	[10]
Ti_3C_2 NDs/S	Nanosheets	67.6/1.8	1609/0.05	950/2.0	1085/400/2.0	0.057	[11]
$Ti_3C_2T_x$/MoS_2-C/S	Nano-hybrids	79/1.0	1195/0.1	677/2.0	799/300/0.5	0.07	[12]
Ti_3C_2@rGO/S	Aerogel	45/1.57	1270/0.1	699/1.0	596/500/1.0	0.07	[13]
$Ti_3C_2T_x$/Meso-C/S	Particle	72.8/2.0	1225/0.05	544/4.0	704/300/0.5	0.142	[14]
S@500-$Ti_3C_2O_x$	Hetero-structure	60/-	1540/0.5	705/5.0	662/1000/1.0	0.08	[15]
S@TiO_2/Ti_2CT_x	Nano-architecture	78/2.0	1408/0.2	576/2.0	464/200/2.0	0.05	[16]
Mo_2C-CNTs/S	Hybrid	87/1.8	1438/0.1	665/5.0	925/250/0.1	0.1	[17]
Mo_2C-C/S	Nano-octahedron	72/1.1	1396/0.1	1050/1.0	762/600/1.0	0.046	[18]

3. Supplementary References

[1] X. Zhao, H. Wang, G. Zhai, G. Wang, *Chem.,* **2017,** *23*, 7037-7045.

[2] H. Zhang, Q. Qi, P. Zhang, W. Zheng, J. Chen, A. Zhou, W. Tian, W. Zhang, Z. Sun, *ACS Appl. Energy Mater.,* **2019**, *2*, 705-714.

[3] M. Chen, Q. Lu, S. Jiang, C. Huang, X. Wang, B. Wu, K. Xiang, Y. Wu, *Chem. Eng. J.,* **2018,** *335*, 831-842.

[4] X.K. Huang, K.Y. Shi, J. Yang, G. Mao, J.H. Chen, *J. Power Sources*, **2017,** *356*, 72–79.

[5] Y. Li, D. Ye, W. Liu, B. Shi, R. Guo, H. Zhao, H. Pei, J. Xu, J. Xie, *ACS Appl. Mater. Interfaces,* **2016,** *8*, 28566-28573.

[6] Q. Jin, L. Li, H. Wang, H. Gao, C. Zhu and X. Zhang, *Electrochimica Acta*, **2019**, 312, 149-156.

[7] W. Bao, X. Xie, J. Xu, X. Guo, J. Song, W. Wu, D. Su, G. Wang, *Chem.,* **2017**, *23*, 12613-12619.

[8] X. Liang, Y. Rangom, C.Y. Kwok, Q. Pang, L.F. Nazar, *Adv. Mater.*, **2017**, *29*, 1603040.

[9] X.T. Gao, Y. Xie, X.D. Zhu, K.N. Sun, X.M. Xie, Y.T. Liu, J.Y. Yu, B. Ding, *Small,* **2018**, *14*, 1802443.

[10] X. Wang, C. Yang, X. Xiong, G. Chen, M. Huang, J.-H. Wang, Y. Liu, M. Liu, K. Huang, *Energy Storage Mater.*, **2019**, 16, 344-353.

[11] Z. Xiao, Z. Li, P. Li, X. Meng, R. Wang, *ACS Nano,* **2019**, *13*, 3608-3617.

[12] Y. Zhang, Z. Mu, C. Yang, Z. Xu, S. Zhang, X. Zhang, Y. Li, J. Lai, Z. Sun, Y. Yang, Y. Chao, C. Li, X. Ge, W. Yang and S. Guo, *Adv. Funct. Mater.*, **2018**, 28, 1707578.

[13] J. Song, X. Guo, J. Zhang, Y.Chen, C. Zhang, L. Luo, F. Wang, G . Wang. *J. Mater. Chem. A.* **2019**; 7, 6507-6513.

[14] W. Bao, D. Su, W. Zhang, X. Guo, G. Wang, *Adv. Funct. Mater.* **2016**, 26, 8746–8756.

[15] H. Pan, X. Huang, R. Zhang, D. Wang, Y. Chen, X. Duan, G. Wen. *Chem. Eng. J.* **2019**, 358, 1253-1261.

[16] C. Du, J. Wu, P. Yang, S. Li, J. Xu and K. Song, *Electrochimica Acta*, **2019**, 295, 1067-1074.

[17] L. P. Lv, C. F. Guo, W. Sun and Y. Wang, *Small*, **2019**, 15, 1804338.

[18] G. Chen, Y. Li, W. Zhong, F. Zheng, J. Hu, X. Ji, W. Liu, C. Yang, Z. Lin, M. Liu, *Energy Storage Mater.*, **2020**, 25, 547-554.